

Quantifying the Cooling Effect of Urban Greening Driven by Ecological Restoration Projects in China

Dong Xu, Tingting Bai,* Lin Yang, Yuyu Zhou, Bin Chen, Haifeng Xu, Yongze Song,* Yuan Yuan, Yuanzheng Cui, Meng Lin, Ziqian Xia, Min Chen, Zhenci Xu, Peng Zhao, Guihua Dong, Lei Zhang, Jiacheng Zhao, Wanben Wu, Wei Wang, Zhao Liu, Jie Cheng,* and Philippe Ciais*



Cite This: <https://doi.org/10.1021/acs.est.4c10314>



Read Online

ACCESS |

Metrics & More

Article Recommendations

Supporting Information

ABSTRACT: Urban greening (UG) affects local climate by altering surface energy balance, while long-term UG cooling potential, patterns, and contribution to curbing urban warming remain unclear. Here, we designed a novel statistical model to evaluate the cooling potential of UG (CPUG) and created the first CPUG map for China. By exploring the trends in observed and simulated urban surface temperatures (UST), we quantified the CPUG of 0.20 K over the past two decades, which slowed down the warming trend by 14.17% in Chinese cities. We found that the CPUG varied significantly between the urban core and sprawl areas. Specifically, the CPUG in the urban core was approximately 1.01 K, and it contributed to curbing urban warming by 56.08%, which was more than 7.2 times higher than in the sprawl areas, where the CPUG was only 0.14 K and contributed to curbing urban warming by 9.93%. We further revealed that urbanization and major ecological restoration projects are the key factors influencing CPUG, emphasizing the need for anthropogenic vegetation management to curb urban warming. The proposed model in this study provides a powerful tool for quantitatively assessing the impact of long-term UG trends on urban warming. The results of the study are an important reference for building climate-adaptive cities.

KEYWORDS: *urban greening, ecological restoration project, cooling effect, climate mitigation*



1. INTRODUCTION

China has experienced a dramatic shift in urbanization, with more than 60% of the population living in urban areas.¹ Over the past two decades, the country's built-up area has increased by over 30,000 km², accounting for approximately 46.67% of the global urban expansion area (Figure S1). Rapid urban expansion has fundamentally altered surface properties and energy balance,² leading to various eco-environmental issues such as air pollution and biodiversity loss, as well as urban warming.³ Moreover, as a result of climate change, the frequency and intensity of extreme heat events in cities have significantly increased, exacerbating the impact on urban natural and socio-economic systems through the compounded effect of the heat island effect and heat waves.^{1,4}

The benefits of urban greening (UG) in improving local climate have been well-documented.^{5,6} UG is known to mitigate global warming through efficient absorption of atmospheric carbon dioxide via photosynthesis⁷ and to alter biophysical properties,^{8,9} such as increasing surface roughness and evapotranspiration, which leads to surface cooling. However, most studies focus on the microclimate impacts of changes in green spaces in urban areas,¹⁰ and do not fully account for the impact of long-term UG trends on the local climate. Estimating

the cooling potential of UG (CPUG) is challenging due to global variability in urban climatic contexts, data sources, and research methods, including manipulation experiments,¹¹ model simulations,⁶ and remote sensing,¹² which often result in diverse and even contradictory results, making it difficult to reveal universal patterns.¹⁰ Understanding persistent and common UG trends can provide an actionable basis for urban warming mitigation strategies. Thus, integrating UG into a national urban surface temperature (UST) mitigation and adaptation strategy remains challenging due to the complexity of biophysical processes, which makes it difficult to separate unidirectional signals of UG affecting local climate from a multitude of potential factors. Consequently, previous studies remain controversial regarding the sign and magnitude of the temperature response to the greening of urban areas.^{13,14}

Received: September 27, 2024

Revised: November 7, 2024

Accepted: November 7, 2024

The effectiveness of UG in curbing urban warming depends on the location of vegetation management intensification.¹⁵ While many studies have documented the extent to which nature-based solutions contribute to climate mitigation, such as carbon sequestration in mangroves¹⁶ and agricultural soils,¹⁷ the carbon metric alone may not fully reflect the climate mitigation potential of these solutions.¹⁸ Integrated assessment models, which generate most mitigation policies and scenarios, ignore the biogeophysical effects of vegetation change.¹⁹ For example, afforestation in the tropics is nearly twice as effective as suggested by carbon accounting alone because evaporative cooling outweighs solar radiation absorption.²⁰ In contrast, the net effect of greening on climate in colder regions of the Northern Hemisphere remains a subject of debate²¹ because previous studies have shown that albedo warming effects dominate in these regions, unlike greening, which is gradual. Despite the ongoing debate, there are currently no studies on the impact of climatic background on the UST mitigation contribution of UG to support its applicability in urban areas. Moreover, ecological restoration projects (ERPs) have helped China contribute to 25% of global greening over the past two decades, but their impact on the contribution of UG to urban warming in Chinese cities has not been effectively quantified.²²

Additionally, UG tends to increase the value of land and property, benefiting elite groups and exacerbating social and environmental inequalities.^{23,24} Consequently, questions arise about whether elite groups have a greater right to enjoy the cooling benefits of UG than working-class and racialized urban dwellers.^{25–27} The lack of national mapping of the UST mitigation contribution of UG in China limits the government's ability to prioritize where to invest to maximize climate benefits, and the potential impact factors and resulting impacts remain unclear. Therefore, to comprehensively understand the cooling potential of UG and its contribution to urban warming on a national scale, a comparative study using consistent methods across time and space is essential.

To address these issues, we conducted long-term continuous monitoring of urban areas in China and designed a simple yet robust model for evaluating the CPUG based on the Normalized Difference Vegetation Index (NDVI) extracted from the Moderate Resolution Imaging Spectroradiometer (MODIS) data product (Figure S2). We report, for the first time, a map of the CPUG in China from 2001 to 2018. Moreover, we examine the spatial gradient of the CPUG with respect to urbanization, exposure, inequality, and other relevant drivers (e.g., ecological restoration project). The contribution (see Text S1 for more details) of this study is to provide convincing evidence of China's efforts to combat global climate change and to emphasize the importance of prioritizing urban ecological restoration, especially in the context of the ongoing discussion on the question, "Do we need to plant trees?".

2. MATERIALS AND METHODS

2.1. Data Sets. This study utilizes multiple data sets, including administrative division data, MOD13A2 normalized vegetation index data,²⁸ MCD12Q1 land cover type data,²⁹ MOD11A2 land surface temperature data,³⁰ MOD09A1 land surface reflectance data,³¹ the ERAS-Land reanalysis data set,³² WorldPop population density data sets,³³ the impervious surface data,³⁴ the harmonized global nighttime light data set,³⁵ Global Urban Boundaries data³⁶ and climate zone data.³⁷

The administrative division data came from the National Catalogue Service for Geographic Information (NCSGI).

MODIS data were obtained from the National Aeronautics and Space Administration (NASA); MOD13A2 and MOD11A1 were used as indicators to evaluate the CPUG on UST, and MCD12Q1 was used as precision verification data for urban boundaries. MOD09A1 was used to calculate the impermeability index (IBI).³⁸ The IBI, MOD13A2, MOD11A1, ERAS-Land reanalysis, WorldPop population density and Harmonized global nighttime light (NTL) data sets were used for sensitivity analysis. CHEQ data were obtained from the National Earth System Science Data Center and used to evaluate the urban eco-environmental benefits brought by UG. Detailed information on the data used in this study is shown in Table S4.

2.2. Method Flowchart. The method flowchart and concept map of this study are shown in Figure S3. The study process comprises five main parts. First, all data were resampled to a 1 km resolution. Second, the Global Urban Boundaries data were combined for all years for maximum value synthesis to extract the LUB and then verified with MCD12Q1 data. Third, we synthesized the annual UI, UG and UST after noise removal by the Savitzky–Golay (SG) filter³⁹ based on the Google Earth Engine (GEE).⁴⁰ Fourth, we mapped the sensitivity of UST (d_{UST}) to a suite of human and natural factors, nighttime light (NTL), the impermeability index (IBI), normalized difference vegetation index (NDVI), population density (POP), 2-m air temperature (TEMP), precipitation (PRE), 10-m wind speed (WIND), solar radiation (SR) and surface pressure (PRES). Fifth, based on the statistical relationship of UST, UG and IBI, that is, Sen_UST, Sen_NDVI and Sen_IBI, we built a model for the assessment of CPUG, in which the Theil-Sen median was used to eliminate the influence of natural factors. Finally, we defined the difference between the simulated Sen_UST (under the no-UG scenario, taking 2001 as the benchmark) and the actual Sen_UST as the CPUG in China from 2001 to 2018.

2.3. LUB Extraction. We used MCD12Q1 to verify the accuracy of the global urban boundaries in China. Figure S4 showed that, except for GUB in 2005, other years are slightly overestimated because the global urban boundaries are clustered by impervious surface data. Overall, the global urban boundaries and MCD12Q1 have good consistency, and the Pearson's r (PCCs) of the four years all exceed 0.85, which is applicable for the extraction of urban boundaries in this study.

We synthesized the maximum value of the global urban boundaries data and delineated all potential urban boundaries in China during this period to precisely quantify the CPUG in China from 2001 to 2018. The calculation formula is as follows:

$$\text{LUB} = \begin{cases} 1 & \text{if } (\exists X_i = 1) \\ 0 & \text{if } (\forall X_i = 0) \end{cases} \quad (1)$$

where the LUB is the largest urban boundary, X_i is the urban boundary of the i th year, and if the pixel value is 1, the pixel is an urban area; otherwise, it is not an urban area.

2.4. IBI Index. The spatial pattern of UST is drastically affected by natural factors and human activities.⁴¹ As mentioned in the introduction, the main natural factors that affect the UST in the spatial dimension are climate, altitude, latitude, and topography. Human activities mainly impact UST through renovation of the underlying surface properties of the urban area, and the most dramatic changes are urban built-up and urban green space.⁴²

In particular, the IBI index was proposed by Xu³⁸ in 2008. Belgian scholars noted that the IBI index has the highest correlation with UST among the 15 remote sensing indices. At

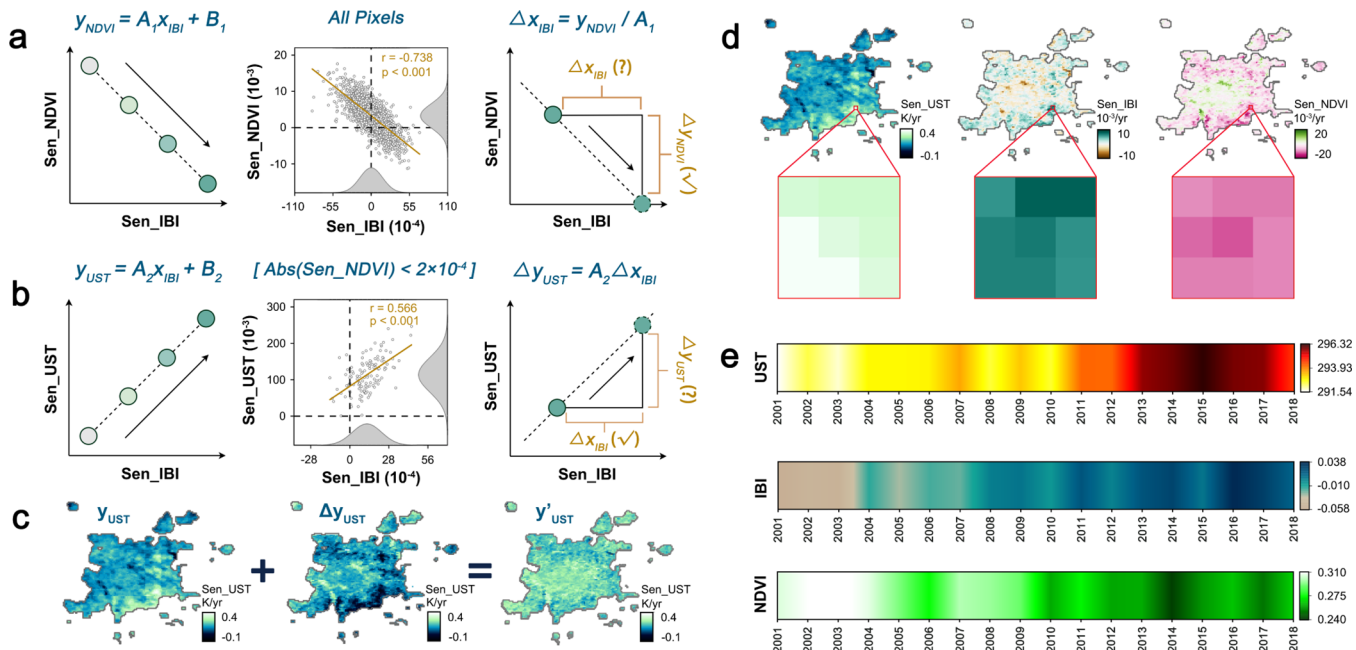


Figure 1. Conceptual diagram for quantifying the CPUG by taking Beijing, China as an example. (a) The linear statistical relationship between UG and UI (Pearson's $r = -0.738, p < 0.001$) in the observation dimension of system time series, and the change in UI under the no-UG scenario. (b) The linear statistical relationship between UI and UST under no-UG scenario (Pearson's $r = 0.566, p < 0.001$) in the observation dimension of system time series. And the change in UST under the no-UG scenario. (c) The calculation process of simulated Sen_UTS. (d) Sen_UTS (light green), Sen_NDVI (magenta), and Sen_IBI (navy blue) values of pixels (3 by 3) in a window in Beijing. The UST and IBI in this region showed a significant upward trend from 2001 to 2018, while the NDVI showed a significant downward trend. (e) Time series heat map of UST, IBI, and NDVI in this window from 2001 to 2018.

the same time, the correlation evaluation between the IBI index and the famous vegetation index NDVI also ranked first and far exceeded the second-placed building index. Therefore, we applied the IBI index to characterize urban impermeability.

In this paper, the MOD09A1 annual average surface reflectance data after cloud removal were used to calculate the IBI index. The calculation formula is as follows:

$$\frac{2 \cdot \text{SWIR}}{(\text{SWIR} + \text{NIR})} - \left[\frac{\text{NIR}}{(\text{NIR} + \text{Red})} + \frac{\text{Green}}{(\text{Green} + \text{SWIR})} \right] \\ \frac{2 \cdot \text{SWIR}}{(\text{SWIR} + \text{NIR})} + \left[\frac{\text{NIR}}{(\text{NIR} + \text{Red})} + \frac{\text{Green}}{(\text{Green} + \text{SWIR})} \right] \quad (2)$$

where SWIR is the shortwave infrared band, NIR is the near-infrared band, Red is the red band, Green is the green band, and IBI is the impermeability index.

2.5. Elimination of the Effects of Natural Factors. As the United Nations Environment Programme noted at the 26th United Nations Climate Change Conference, the sharp rise in UST is caused by the reduction of UG and the expansion of urban impervious surfaces.⁴² Natural factors such as climate, altitude, latitude, and topography cannot change significantly in a short period of time. Therefore, we believe that the Theil-Sen median^{43,44} trend can effectively eliminate the effects of natural factors on the UST in the system time series dimension from 2001 to 2018.

The Theil-Sen median trend is a rank-based nonparametric test. Its advantage lies in the ability to test linear or nonlinear trends.^{43,44}

$$S = \sum_{i=1}^{n-1} \sum_{j=i+1}^n \text{sgn}(X_j - X_i) \quad (3)$$

where X_i and X_j are the values corresponding to years i and j in the system time series, respectively, and n is the length of the time series data.

As found in previous studies,⁴⁵ the main factors affecting UST in the spatial dimension include natural factors and human activities. We recognize the conclusion of the United Nations Environment Programme (that is, the sharp rise in UST is caused by the reduction of UG and the expansion of urban impervious surfaces) in the systematic time dimension. To prove this speculation, we combined multisource remote sensing data with ERA5-land reanalysis data and selected 9 variables, NTL, IBI, NDVI, POP, TEMP, PRE, WIND, SR and PRES, to explore the sensitivity of natural factors and human activity factors to UST (Y_{UST}) from systematic time series observations. We analyzed the multiple regression pixel-by-pixel based on the partial least-squares regression of 9 variables and normalized the regression coefficients by the standard deviation of each variable. All variables were standardized, so they were unitless and comparable.

$$Y_{UST} = b_1 \cdot X_{NTL} + b_2 \cdot X_{IBI} + b_3 \cdot X_{NDVI} + b_4 \cdot X_{POP} \\ + b_5 \cdot X_{TEMP} + b_6 \cdot X_{PRE} + b_7 \cdot X_{WIND} + b_8 \cdot X_{AIR} \\ + b_9 \cdot X_{PRES} + C \quad (4)$$

$$Z_j = b_j \times (S_{X_j} / S_{UST}) \quad (5)$$

where b_j is the fitting coefficient between different variables and UST, while C is the fitting constant. Z_j denotes the sensitivity of UST toward the j -th variable. S_{X_j} and S_{UST} are the standard deviation of the j th variable and UST, respectively.

2.6. A Conceptual Model for Assessing the CPUG. To systematically quantify the impact of UG on urban warming, we

first proposed a theoretical framework and provide the necessary definitions for some parameters. The United Nations (UN) Handbook⁴² has shown that a combination of declining vegetation and increasing impervious surfaces is contributing to the rise in urban surface temperature (UST). Moreover, numerous studies^{46,47} have recognized remote sensing-based vegetation indices, such as the Normalized Difference Vegetation Index (NDVI) or Enhanced Vegetation Index (EVI), as credible indicators of UG growth status. In this model, NDVI, impermeability index (IBI),³⁸ urban land surface temperature are used to characterize UG, UI, UST and their statistical relationships are used to assess the CPUG in China. Conceptually, the CPUG in a time series can be defined as the difference between the UST trend in the no-UG scenario and the actual UST.

$$\text{CPUG} = (\text{Sen_UST}_{\text{no-UG}} - \text{Sen_UST}_{\text{obs}}) \cdot n \quad (6)$$

where $\text{Sen_UST}_{\text{no-UG}}$ is the no-UG scenario UST trend based on the Theil-Sen Median, $\text{Sen_UST}_{\text{obs}}$ is the observed UST trend based on the Theil-Sen Median, and n is the number of years.

Specifically, the concept of CPUG is extended from a single pixel to all pixels in urban by designing a no-UG scenario based on the system time series dimension, setting the NDVI trend (Sen_NDVI) of a pixel to zero and calculating the change in the UST trend (Sen_UST) (in eq 1) based on the difference between the no-UG scenario IBI trend (Sen_IBI) and the observed one (Figure 1).

First, all pixels as samples fit the linear statistical relationship between Sen_NDVI and Sen_IBI . Based on this functional relationship, we calculated the difference between the no-UG scenario and the observed Sen_IBI , i.e., Δx_{IBI} (Figure 1a).

$$y_{\text{Sen_NDVI}} = A_1 x_{\text{Sen_IBI}} + B_1 \quad (7)$$

$$\Delta x_{\text{Sen_IBI}} = y_{\text{Sen_NDVI}} / A_1 \quad (8)$$

where $x_{\text{Sen_IBI}}$ and $y_{\text{Sen_NDVI}}$ are the Sen_IBI and Sen_NDVI of the pixel, respectively. A_1 and B_1 are the coefficients of the linear fit.

Second, we selected pixels under the no-UG scenario (that is, pixels whose Sen_NDVI is between -0.0002 and 0.0002) as samples to fit the linear statistical relationship between Sen_IBI and Sen_UST . Based on the functional relationship and Δx_{IBI} , we calculated the difference between the simulated and the observed Sen_UST , i.e., $\Delta y_{\text{Sen_UST}}$ (Figure 1b). For the statistical relationship at the national scale, see Figure S5.

$$y_{\text{Sen_UST}} = A_2 X_{\text{Sen_IBI}} + B_2 \quad (9)$$

$$\Delta y_{\text{Sen_UST}} = A_2 \Delta x_{\text{Sen_IBI}} \quad (10)$$

where $y_{\text{Sen_UST}}$ is the Sen_UST value of the pixel. A_2 and B_2 are the coefficients of the linear fit. For the threshold selection criteria and their robustness, see Text S2.

Third, the observed Sen_UST was added to $\Delta y_{\text{Sen_UST}}$ to obtain the no-UG scenario Sen_UST , which is the trend of UST without the interference of UG (Figure 1c).

$$y'_{\text{Sen_UST}} = y_{\text{Sen_UST}} + \Delta y_{\text{Sen_UST}} \quad (11)$$

$$\Delta T = n \cdot \Delta y_{\text{Sen_UST}} \quad (12)$$

where $y'_{\text{Sen_UST}}$ is the no-UG scenario Sen_UST , ΔT is the CPUG, and n is the number of years.

Specifically, Sen_NDVI and Sen_IBI showed a significant negative correlation ($p < 0.001$). Similarly, Sen_UST and Sen_IBI showed a significant positive correlation ($p < 0.001$) under the no-UG scenario. This relationship is depicted visually through a 3 by 3 window within the Beijing urban area (Figure 1d). In the systematic time series dimension, the NDVI showed a fast-decreasing trend, while the IBI showed a steadily increasing trend and so does the UST, which supports the conclusions presented in the handbook and previous studies.^{42,48,49} Further, we can apply the model to all urban pixels in China and also to urban pixels in each city in China (and finally, synthesize the results for these cities) to estimate the CPUG in China during 2001–2018. The UST sensitivity analysis for the cluster scale is shown in Figure S6.

2.7. Contribution of UG to Curbing Urban Warming.

The trend of UST (δUST) were calculated by Theil-Sen median ($\delta \text{UST}_{\text{OBS}}$) and simulated ($\delta \text{UST}_{\text{SIM}}$) by the framework in order to assess the UST mitigation effects of biophysical feedbacks of UG. Specifically, the mitigation contribution rate can be expressed as the ratio of the greening-induced UST trend to the rate of urban warming without greening mitigation.

$$\begin{aligned} \text{CR} &= -\frac{\delta \text{UST}_{\text{UG}}}{\delta \text{UST}_{\text{OBS}} - \delta \text{UST}_{\text{UG}}} \times 100\% \\ &= -\frac{\delta \text{UST}_{\text{OBS}} - \delta \text{UST}_{\text{SIM}}}{\delta \text{UST}_{\text{SIM}}} \times 100\% \end{aligned} \quad (13)$$

where CR is the UST mitigation contribution rate of UG, $\delta \text{UST}_{\text{UG}}$ is the greening-induced UST trend, $\delta \text{UST}_{\text{OBS}}$ is the observed UST trend from satellite, and $\delta \text{UST}_{\text{SIM}}$ is the simulated UST trend from the framework.

2.8. Direct and Indirect Effects of Urbanization on Vegetation. The direct and indirect effects of urbanization on vegetation can be quantified using a conceptual framework.⁵ The direct effect is attributed to the increase in urban impermeability (β), which results in a decrease in vegetation indices (e.g., EVI). Thus, in an ideal state, there exists a linear relationship between EVI and β . This linear relationship is defined as the zero-impact line that disregards indirect effects.

$$V_{zi} = (1 - \beta)V_v + \beta V_{nv} \quad (14)$$

where V_{zi} is the theoretical EVI, V_v and V_{nv} are the mean EVI of all pixels that are entirely covered by vegetation ($\beta = 0$) and built-up surfaces ($\beta = 1$), respectively.

Hence, the direct effect of urbanization on vegetation can be calculated using the formula below.

$$\omega_d = \frac{V_{zi} - V_v}{V_v} \times 100\% \quad (15)$$

where ω_d is the direct effect of urbanization.

In fact, not all pixel distributions align exactly along the line established by formula 14. This deviation is attributed to the effect of urbanization that results from the urban location and background climate, which affect vegetation health. Therefore, the indirect effect of the urbanization on vegetation can be measured using the relative change between theoretical and observed EVI values of individual pixels.

$$\omega_i = \frac{V_{obs} - V_{zi}}{V_{zi}} \times 100\% \quad (16)$$

where ω_i is the indirect effect of urbanization and V_{obs} is the observed EVI by the satellite.

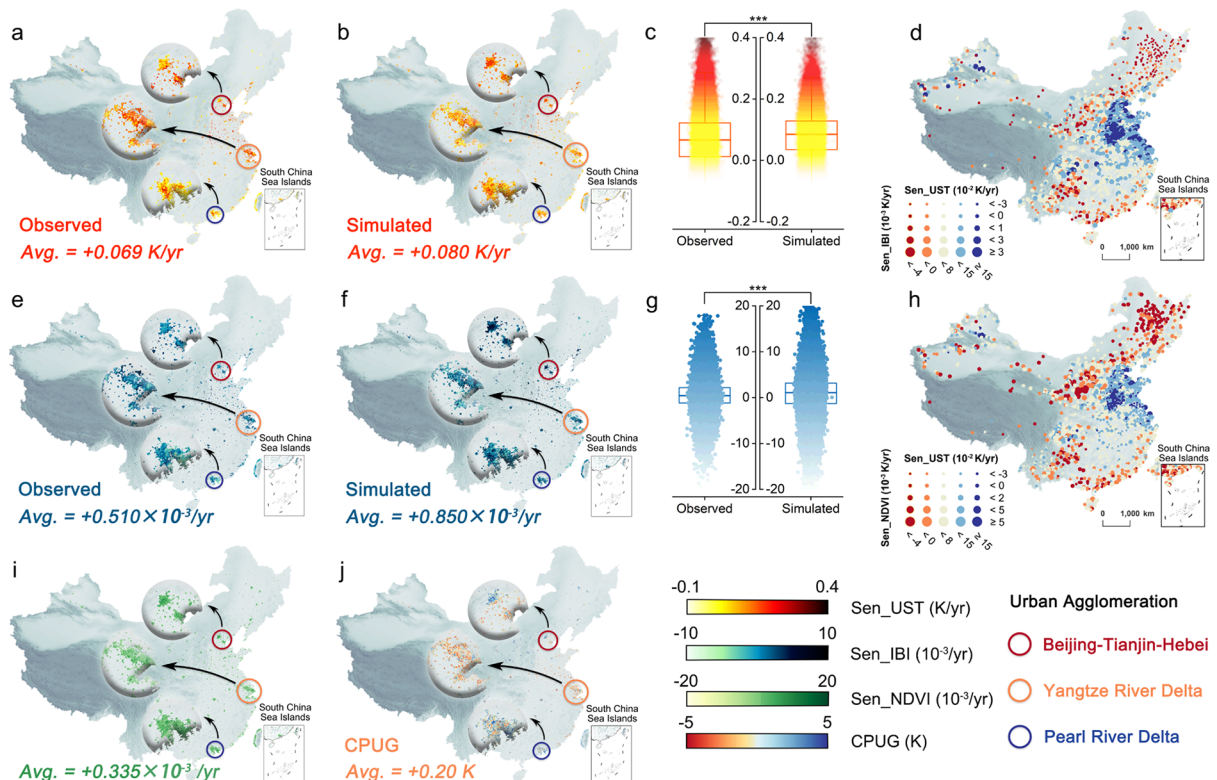


Figure 2. The CPUG map in China from 2001 to 2018 at the 1000-m grid cell scale. (a) Observed Sen_UTST in China from 2001 to 2018. (b) Simulated Sen_UTST in China from 2001 to 2018. (c) Box plot of observed and simulated Sen_UTST. (d) The spatial relationship between Sen_UTST and Sen_IBI at cluster scale. (e) Observed Sen_IBI in China from 2001 to 2018. (f) Simulated Sen_IBI in China from 2001 to 2018. (g) Box plot of observed and simulated Sen_IBI. (h) Distribution map of the spatial relationship between Sen_UTST and Sen_NDVI at cluster scale. (i) The trend of UG in China from 2001 to 2018. (j) The CPUG in China from 2001 to 2018. “***” represents a significant difference between the two groups of samples at least at the 1% level.

3. RESULTS

3.1. The CPUG Map of China during 2001–2018. UG has shown an upward trend over the past two decades in China. The average greening trend for the nation was approximately $0.33 \pm 4.40 \times 10^{-3}/\text{yr}$ (mean \pm a STD of all pixels, as shown in Figure 2i). Out of the 1804 urban clusters with an area greater than 10 km^2 , 1041 urban clusters (57.71%) had a Sen_NDVI greater than 0 (Figure 2h). At the national scale, the simulated UST (Sen_UTST) (Figure 2b) and urban impermeability trend (Sen_IBI) (Figure 2f) were slightly higher than those based on remote sensing observations (for the statistical relationship at the national scale, see Figure S5). The national average Sen_UTST and Sen_IBI increased by $1.13 \pm 11.20 \times 10^{-2} \text{ K}/\text{yr}$ (Figure 2a) and $3.40 \pm 45.94 \times 10^{-3} \text{ yr}$ (Figure 2e), respectively, in the no-UG scenario (taking 2001 as the benchmark). This indicates that UG inhibited UI by $6.18 \pm 82.69 \times 10^{-3}$ and reduced UST by approximately $0.20 \pm 2.02 \text{ K}$ (Figure 2j) nationwide, demonstrating that UG not only had a widespread positive impact on local climate but also had a significant impact on urban gray space (Text S3).

Spatially, areas with high CPUG include Beijing-Tianjin-Hebei (BTH), Yangtze River Delta (YRD), Pearl River Delta (PRD) urban agglomeration (Figure 2a,b,e,f,i,j), Taiwan and other areas with high urbanization levels, as well as the Northwest and Northeast regions represented by Aksu, Karamay, and Shenyang City. The North China Plain and the lower Yangtze River Plain have the lowest CPUG (Figure 2j), despite having the fastest rising UI and UST with a medium level of urbanization. Further, the analysis suggests that the drivers of

the spatial gradient pattern of CPUG may be complex and diverse and not solely dependent on the urbanization level.

We further evaluated the CPUG of 79 cities with an area larger than 500 km^2 (Figure S7). The accuracy was validated against simulated results based on common relationships, as shown in Figure S8. Information for each index of these cities was recorded and listed in descending order according to the CPUG (Table S3). Over the past two decades, the UG in 42 cities had a cooling potential ($\text{Sen}_\text{NDVI} > 0$), primarily located in the North China region (including the Loess Plateau, BTH urban agglomeration, Xinjiang, Northeast China) and the PRD urban agglomeration. Karamay had the highest CPUG, reaching $2.25 \pm 2.80 \text{ K}$ (detailed explanation can be found in Text S4), followed by three National Forest Cities: Anshan ($2.09 \pm 2.50 \text{ K}$), Liaoyang ($1.99 \pm 2.40 \text{ K}$), and Shenyang ($1.77 \pm 2.66 \text{ K}$) (Figure S9a). In contrast, cities with CPUG < 0 were mainly concentrated in the eastern coastal areas, as shown in Figure S7.

We also selected 15 representative cities located in different climatic zones of China to demonstrate the microspatial patterns of the CPUG at the city scale. The CPUG assessment model was fitted to each city (Figure S10). The CPUG maps of the 15 representative cities (detailed locations can be found in Figure S11) are shown in Figures S12 and 13. Among the 15 cities, UG in 9 cities had a positive impact on local cooling. Furthermore, similar to Sen_UTST, the simulated Sen_IBI was higher than the observed Sen_IBI for these cities (Figure S14). Although six cities had an overall CPUG of less than 0, their spatial distribution patterns showed a significant cooling effect in the urban core area of these cities.

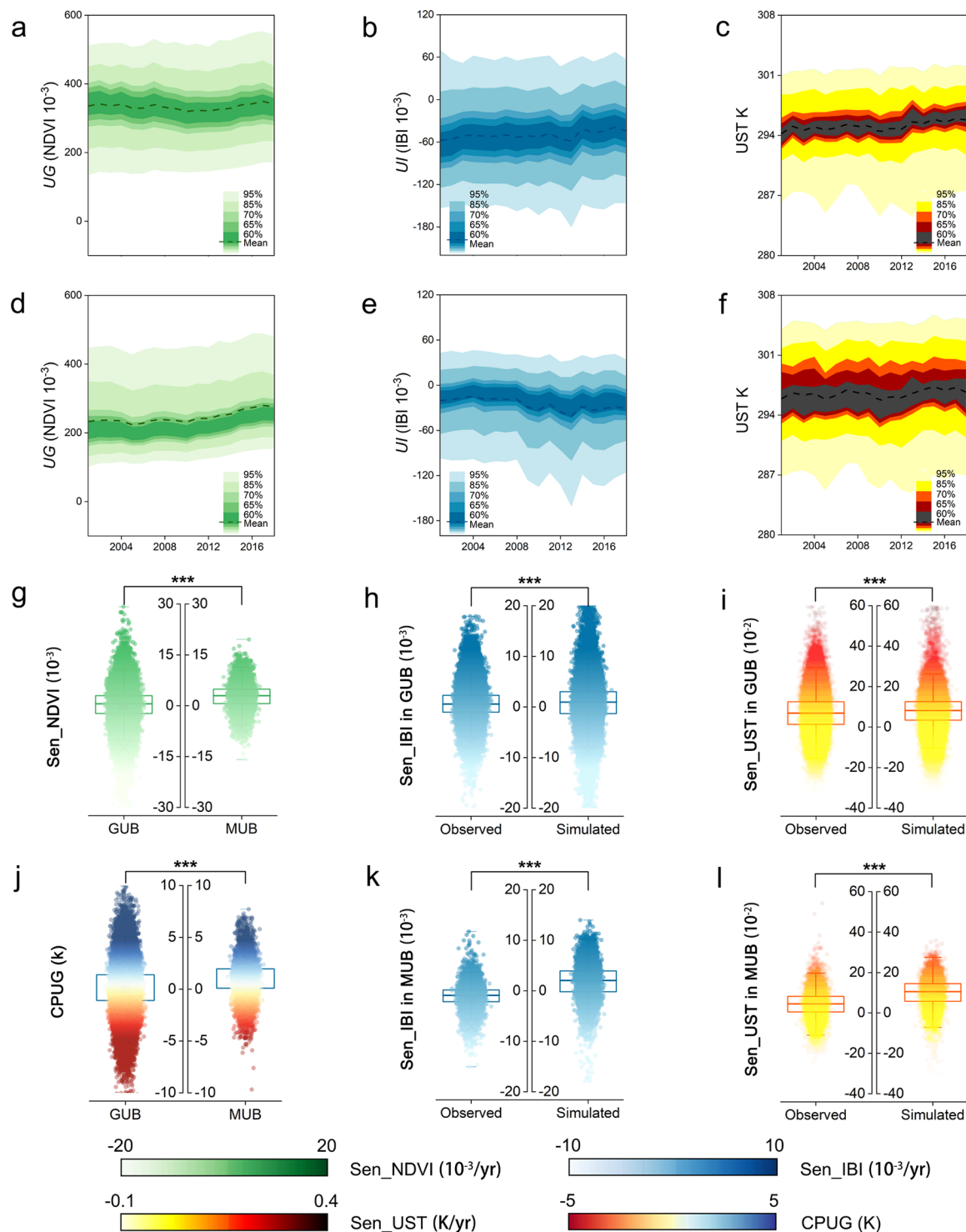


Figure 3. Box plots of Sen_IBI (observed, simulated), Sen_UST (observed, simulated), and Sen_NDVI of the GUB and MUB. Time series diagrams of UI and UG in the GUB and MUB between 2001 and 2018. (a) Observed and simulated Sen_IBI in the GUB. (b) Observed and simulated Sen_IBI in the MUB. (c) Observed and simulated Sen_UST in the GUB. (d) Observed and simulated Sen_UST in the MUB. (e) Sen_NDVI in the GUB and MUB. (f) Time series diagram of UI in the GUB. (g) Time series diagram of UI in the MUB. (h) Time series diagram of UG in the GUB. (i) Time series diagram of UG in the MUB. “***” represents a significant difference between the two groups of samples at least at the 1% level.

3.2. Anisotropy of CPUG in Urban Core-Sprawl Areas.

We observed a consistent and interesting phenomenon that the CPUG in the main urban boundaries (MUB), which constitute the urban core, is higher than that in the grown urban boundaries (GUB), resulting in a “Fried Egg”^{50,51} spatial distribution pattern (Figure S15). The area resembling the

“yolk” has a higher CPUG, which aligns with the spatial distribution pattern of Sen_NDVI . This observation may be attributed to the stage of urban development.^{24,52} Specifically, in developing regions, UG policies are primarily concentrated in highly urbanized core areas, as seen in a specific case illustrated in Figure S16.

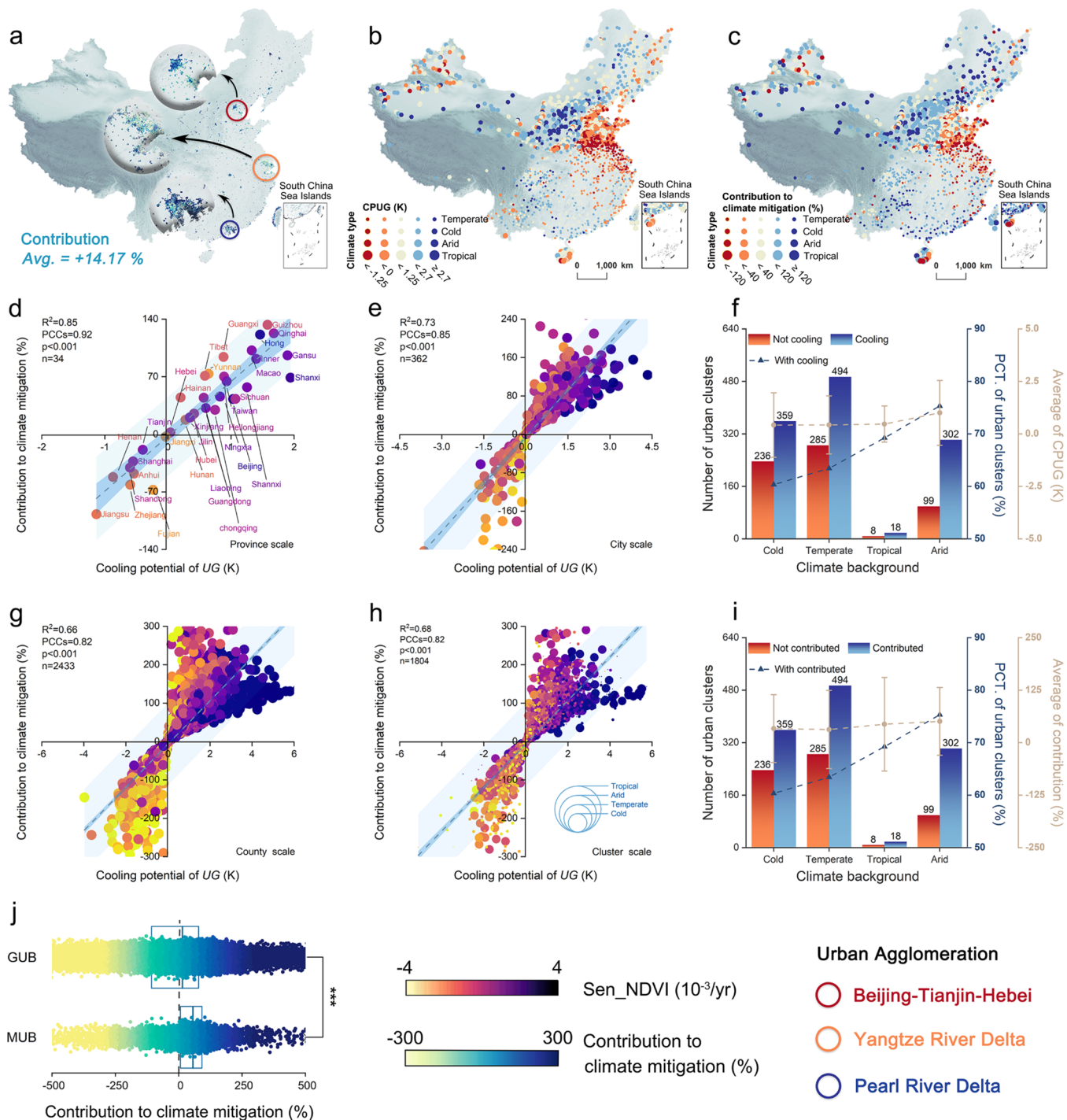


Figure 4. The UG contribution to curb urban warming. (a) The map of UG contribution to curb urban warming at the 1000-m grid cell scale. (b) Spatial distribution map of CPUG in different types of climatic backgrounds at the cluster scale. (c) Spatial distribution of UG contribution to curb urban warming in different climatic backgrounds at the cluster scale. (d) The relationship between CPUG and contribution to curbing urban warming at the provincial scale. (e) The relationship between CPUG and contribution to curbing urban warming at the city scale. (f) The statistical relationship between climate background and CPUG. (g) The relationship between CPUG and contribution to curbing urban warming at the county scale. (h) The relationship between CPUG and contribution to curbing urban warming at the cluster scale in the climate background. (i) The statistical relationship between climate background and contribution to curbing urban warming. (j) The statistical relationship between climate background and contribution to curbing urban warming. Note: “PCT.” is an abbreviation for “Percentage”.

Figure 3 demonstrates the heterogeneity of CPUG in the MUB and GUB, revealing that the trend of vegetation greening in the MUB area ($2.76 \pm 3.46 \times 10^{-3}/\text{yr}$) is much greater than that in the GUB ($0.13 \pm 4.41 \times 10^{-3}/\text{yr}$) (Figure 3g). The vegetation greening in the MUB shows a rapid upward trend

(Figure 3d), while that in the GUB displays a U-shaped characteristic (Figure 3a); which can be explained by the Environmental Kuznets Curve (EKC).⁵³ In particular, the urbanization of the MUB area reached a mature stage during 2001–2018, whereas the GUB is still in the stage of rapid

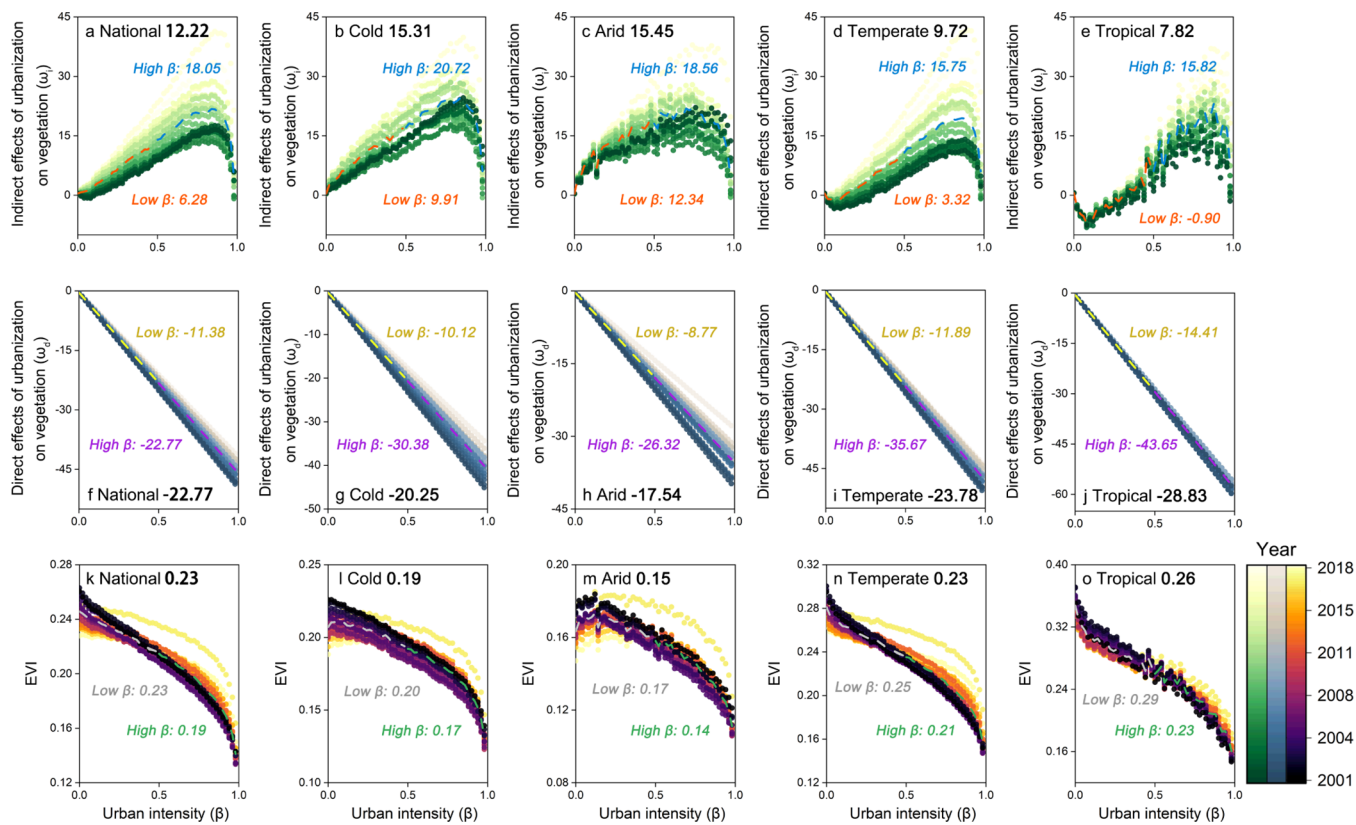


Figure 5. Direct (ω_d) and indirect (ω_i) effects of urbanization on vegetation in China from 2001 to 2018 in the climate background. (a–e) Indirect effects of urbanization on vegetation. (f–j) Direct effects of urbanization on vegetation. (k–o) The relationship between EVI and urbanization.

development. Hence, residents of the MUB have more pressing needs for a high-quality living environment, forcing managers to implement more UG projects.⁵⁴ In addition, the observed Sen_IBI of the GUB ($0.64 \pm 2.87 \times 10^{-3}/\text{yr}$) was higher than that of the MUB ($-1.09 \pm 2.12 \times 10^{-3}/\text{yr}$) (Figure 3h,k), indicating that the impermeability of the MUB decreased over the past two decades (Figure 3e), while that of the GUB area has minutely increased (Figure 3b). The simulated Sen_IBI of the GUB ($0.78 \pm 3.68 \times 10^{-3}/\text{yr}$) was lower than that of the MUB ($1.79 \pm 3.14 \times 10^{-3}/\text{yr}$), and the difference between the simulated and observed Sen_IBI of the GUB ($0.14 \pm 4.24 \times 10^{-3}/\text{yr}$) was much smaller than that of the MUB ($2.88 \pm 3.62 \times 10^{-3}/\text{yr}$).

Similarly, the observed Sen_UTS of the GUB ($7.06 \pm 8.56 \times 10^{-2} \text{ K}/\text{yr}$) was higher than that of the MUB ($4.39 \pm 6.29 \times 10^{-2} \text{ K}/\text{yr}$) (Figure 3i,l). The simulated Sen_UTS of the GUB ($7.84 \pm 3.68 \times 10^{-2} \text{ K}/\text{yr}$) was lower than that of the MUB ($9.98 \pm 6.64 \times 10^{-2} \text{ K}/\text{yr}$). The difference between the simulated and observed Sen_UTS of the GUB ($0.78 \pm 10.85 \times 10^{-2} \text{ K}/\text{yr}$) was much smaller than that of the MUB ($5.59 \pm 8.51 \times 10^{-2} \text{ K}/\text{yr}$). The CPUG in the MUB ($1.01 \pm 1.53 \text{ K}$) was 7.2 times greater than that in the GUB ($0.14 \pm 1.95 \text{ K}$), indicating that the CPUG in developed regions is more prominent than that in developing regions, which further confirms our above findings and further proving the validity of the EKC.

We further analyzed the relationship between urban expansion rates and CPUG at the provincial, city, and county scales from 2001 to 2018 (Figure S17). We revealed that, at all scales, CPUG is significantly negatively correlated with the speed of urban expansion. Additionally, we tallied the number of provinces, cities, and counties with CPUG greater than or less

than 0, and found that more than 60% of these regions had a CPUG greater than 0 in both MUB and GUB. Furthermore, we observed that, across different scales, the proportion of regions with a CPUG greater than 0 was higher in MUB than in GUB. This suggests that a higher level of spatial urbanization has a positive impact on the CPUG spatial gradient pattern.

3.3. Contribution of UG to Curbing Urban Warming. At a national level, UG has curbed the warming trend by 14.17% over the past two decades (Figure 4a), which is much higher than the 4.6% reported in a recent study.⁵⁵ Impressively, UG contributed 56.08% to the reduction of urban warming in the MUB and 9.93% in the GUB areas. The high contribution areas at a national level were mainly located in the urban agglomerations of BTH (10.29%), YRD (-68.92%), and PRD (46.11%) (Figure 4a). At the regional scale, the areas that significantly curb urban warming are mainly located in northern China, including the Loess Plateau, the Northwest Arid Zone, and the Northeast (Figure 4c), which is consistent with the spatial distribution pattern of the CPUG (Figure 4b). Furthermore, we observed a significant positive relationship between CPUG and the contribution of UG in curbing urban warming at different scales (Figure 4d,e,g,h). Of the four climate zones, the arid zone had the highest CPUG and its contribution to reducing urban warming was 1.00 K and 50.63%, respectively (Figure 4f,i). These results suggest that UG has a more widespread positive effect on local climate in regions with limited water availability, which is contrary to the conclusions reached in a recent study.⁵⁶

4. DISCUSSION

Cities have long been known as “growth machines” and now contribute to 90% of global GDP, yet they also account for 75% of global carbon emissions,²³ and urban warming rates is twice the global average.⁴² The Paris Agreement aims to limit the global warming trend to 1.5 °C,⁵⁷ and cities, as “natural laboratories” for global climate change,⁵ must develop a generic cooling strategy to curb their warming trends. This is especially important given rapid urbanization,¹⁹ dramatic climate change,⁵⁸ and frequent climate extremes.⁵⁹ Furthermore, previous studies that used carbon metrics to evaluate the UST mitigation potential of greening have been subject to significant uncertainties, particularly in urban areas.⁶⁰ Therefore, it is necessary to use surface temperature sensitivity to quantify the UST mitigation potential of UG, which effectively integrates the biogeochemical and biophysical effects of vegetation. Therefore, the study presents a quantitative assessment model of the long-term impact of UG on curbing urban surface warming. By mapping the benefits of implementing UG, it can assist governments in prioritizing investments to maximize climate benefits.

Overall, the study provides compelling evidence that long-term UG has effectively curbed urban warming in China by 14.17% over the past two decades, a figure that exceeds any previous study.^{55,61} Specifically, we found that UG contributed a staggering 56.08% to curbing urban warming in the MUB, compared to 9.93% in the GUB. This phenomenon can be attributed to the direct (negative) and indirect (positive) effects of urbanization on vegetation,²⁴ as depicted in Figure 5. The figure shows that the indirect effects of urbanization on vegetation increase with increasing impermeability (β) (Figure 5a–e), while the indirect and direct effects of urbanization on vegetation increase and decrease with the increasing year (Figure 5a–j), respectively, in different climatic zones. We revealed that the indirect effects were higher in areas with high urbanization levels ($\beta > 0.5$), while the direct effects were lower. Here, the promoting effect of urbanization on vegetation is mainly reflected in the intensive management of urban vegetation rather than the greenhouse effect of carbon dioxide (see Text S5). This underscores the importance of considering the level of urbanization as a critical factor influencing the climatic effects of the CPUG and provides valuable insight into where trees should be planted to achieve the maximum climate benefits.¹³ Nonetheless, we also discovered that significant disparities in urbanization between core-sprawl areas resulted in substantial inequalities in CPUG exposure. Regions with higher income, resource consumption, and pollution emissions were more susceptible to CPUG, affecting a population of 506 million people (detailed explanation see Text S6). This highlights the need for policymakers to consider the trade-offs and synergies between developing urban warming solutions and promoting social equity to build inclusive, safe, resilient, and sustainable cities.⁶²

On the other hand, our study provides evidence that UGs in cities associated with ecological restoration projects (ERPs) have significant UST mitigation potential,^{63–65} except in highly urbanized areas (Figures S12–14). To quantify the impact of ERPs on CPUG, we present a high-precision Chinese ecological quality assessment model (Text S6) and provide empirical statistical evidence (Figure S18). Our findings suggest that ERPs not only promote the greening of forest vegetation but also contribute to CPUG (Text S8 and Figure S19), providing new

evidence for the recent controversy surrounding this issue.^{14,66} By improving our understanding of the mechanisms by which ERPs influence the distribution patterns of CPUG across the country, our study demonstrates the potential of ERPs for future adaptation to continuing global urban warming trends.

In brief, this study introduces a solid model to assess the impact of long-term greening on local cooling. The model results reveal general patterns of UG on local cooling and quantify the contribution of CPUG to urban warming in China over the past 20 years, and further highlight the need for effective management of urban vegetation as a climate mitigation strategy. This study improves transparency in accounting for the climate benefits of UG at a national scale, and the proposed model can be widely applied to other regions of the world to assess the UST mitigation impacts of implementing nature-based solutions.

The study has some caveats that should be mentioned. First, quantifying spatial variations in urban green space density, compactness, and spread shape using NDVI data is challenging, and different green space structures may lead to complex differences in CPUG. Moreover, other environmental factors, such as tree species composition, air pollutants, and nitrogen deposition, can also influence the growth of urban vegetation. Additionally, while NDVI retains the same change trend compared to other vegetation indices (Figure S20), differences between vegetation indices can also affect CPUG. Second, the analysis only quantifies the empirical statistical impact of UG on local cooling and ignores biophysical feedback mechanisms. Finally, satellite observations of surface temperatures were used as thermal conditions, but near-surface air temperatures may be more relevant to human living conditions. However, obtaining air temperature estimates often requires complex assimilation methods or statistical models combined with in situ observations, which can result in potentially large data uncertainties.⁶⁷ Most earth system models lack the ability to describe the direct role of humans in regional greening in complex model inference,²² which makes the air temperature data based on earth system models may not be able to objectively reveal the cooling effect of vegetation due to human land use practices. Therefore, multidomain cross-collaborative studies are necessary once high-resolution data on these factors become available on a global scale.

ASSOCIATED CONTENT

Data Availability Statement

China’s CPUG data set and China’s high-resolution eco-environmental quality data from 2001 to 2018 can be obtained from the National Earth System Science Data Center (<https://www.geodata.cn/>). Other data sets used in this study are available upon request and were obtained from public data sources or provided by the original data producers (authors).

Supporting Information

The Supporting Information is available free of charge at <https://pubs.acs.org/doi/10.1021/acs.est.4c10314>.

Research contribution (Text S1); threshold robustness assessment (Text S2); association of urban heatness, greenness and grayness at the cluster scale (Text S3); case studies of major cities (Text S4, Figures S7, S11–14, S16); contribution of urbanization to urban greening is reflected in the intensified management of vegetation (Text S5); Inequality in the exposure of CPUG (Text S6); evaluation of EEQ (Text S7, Figures S18–S19);

potential impact of ERPs on CPUG (Text S8); rate of urbanization in China (Figure S1); spatial distribution maps of NDVI and UST trends (Figure S2); method flowchart (Figure S3); model robustness validation (Figures S4–S6, S8–S10, S20); heterogeneity of urban elements and CPUG in core-sprawl areas (Figure S15); the impact of urban sprawl on CPUG (Figure S17) ([PDF](#))

Accession Codes

In order to enhance the efficiency of CPUG calculations, we developed a Node.js and ML.js-based program for quantitative evaluation of the impact of UG on UST. This program enables convenient simulation of UST changes in various cities across the globe. The ultimate goal of this research is to encourage fellow scholars to further investigate this topic in greater detail. The program code can be accessed at <https://github.com/codeOH/simulated.git>. The code for data collection is available at <https://zenodo.org/record/7979211>.

AUTHOR INFORMATION

Corresponding Authors

Tingting Bai – School of Business Administration, Northeastern University, Shenyang 110189, China; Email: Baitingting27@163.com

Yongze Song – School of Design and the Built Environment, Curtin University, Perth 6102, Australia; Email: yongze.song@curtin.edu.au

Jie Cheng – State Key Laboratory of Remote Sensing Science, Faculty of Geographical Science, Beijing Normal University, Beijing 100875, China; Key Laboratory of Environmental Change and Natural Disasters of Ministry of Education, Beijing Normal University, Beijing 100875, China; Email: Jie_Cheng@bnu.edu.cn

Philippe Ciais – Laboratoire des Sciences du Climat et de l'Environnement, CEA CNRS UVSQ, Gif-sur-Yvette 91191, France; Email: philippe.ciais@cea.fr

Authors

Dong Xu – Department of Geography, National University of Singapore, Singapore 119077, Singapore; State Key Laboratory of Remote Sensing Science, Faculty of Geographical Science, Beijing Normal University, Beijing 100875, China; Key Laboratory of Environmental Change and Natural Disasters of Ministry of Education, Beijing Normal University, Beijing 100875, China; [orcid.org/0009-0002-8238-2665](#)

Lin Yang – School of Geography and Ocean Science, Nanjing University, Nanjing 210023, China

Yuyu Zhou – Institute for Climate and Carbon Neutrality, The University of Hong Kong, Hong Kong SAR 999077, China; Department of Geography, The University of Hong Kong, Hong Kong 999077, China

Bin Chen – Future Urbanity & Sustainable Environment (FUSE) Lab, Division of Landscape Architecture, Department of Architecture, Faculty of Architecture, The University of Hong Kong, Hong Kong SAR 999077, China; [orcid.org/0000-0003-3496-2876](#)

Haifeng Xu – School of Information Science and Technology, Beijing Forestry University, Beijing 100083, China

Yuan Yuan – Department of Environmental Science and Engineering, Fudan University, Shanghai 200438, China

Yuanzheng Cui – Key Laboratory of Watershed Geographic Sciences, Nanjing Institute of Geography and Limnology, The Chinese Academy of Sciences, Nanjing 210008, China; College

of Geography and Remote Sensing, Hohai University, Nanjing 210098, China; [orcid.org/0000-0001-9013-3568](#)

Meng Lin – Department of Earth and Environmental Sciences, Vanderbilt University, Nashville, Tennessee 37235, United States

Ziqian Xia – School of Economics and Management, Tongji University, Shanghai 200092, China

Min Chen – Key Laboratory of Virtual Geographic Environment (Ministry of Education of PRC), Nanjing Normal University, Nanjing 210023, China

Zhenci Xu – Department of Geography, The University of Hong Kong, Hong Kong 999077, China

Peng Zhao – Key Laboratory of Mountain Hazards and Earth Surface Processes, Institute of Mountain Hazards and Environment, Chinese Academy of Sciences, Chengdu 610041, China

Guizhong Dong – State Environmental Protection Key Laboratory of Quality Control in Environmental Monitoring, China National Environmental Monitoring Centre, Beijing 100012, China

Lei Zhang – School of Geography and Ocean Science, Nanjing University, Nanjing 210023, China

Jiacheng Zhao – School of Ecology and Applied Meteorology, Nanjing University of Information Science and Technology, Nanjing 210044, China; [orcid.org/0000-0002-1493-4723](#)

Wanben Wu – Ministry of Education Key Laboratory for Biodiversity Science and Ecological Engineering, National Observations and Research Station for Wetland Ecosystems of the Yangtze Estuary, and Shanghai Institute of EcoChongming (SIEC), Fudan University, Shanghai 200433, China

Wei Wang – School of Urban and Environmental Studies, Northwestern University, Xi'an 710069, China

Zhao Liu – School of Geography, Planning and Spatial Sciences, University of Tasmania, Hobart TAS 7005, Australia

Complete contact information is available at:
<https://pubs.acs.org/10.1021/acs.est.4c10314>

Notes

The authors declare no competing financial interest.

ACKNOWLEDGMENTS

This work was partly supported by the National Natural Science Foundation of China via grant 42071308. Thanks to the Ministry of Ecology and Environment of the People's Republic of China for providing the National County ecological index data. Thanks to the National Earth System Science Data Center for providing us with data release services.

REFERENCES

- (1) Yang, X. J. China's rapid urbanization. *Science* **2013**, *342* (6156), 310–310.
- (2) Schneider, A.; Friedl, M. A.; Potere, D. Mapping global urban areas using MODIS 500-m data: New methods and datasets based on 'urban ecoregions'. *Remote Sens. Environ.* **2010**, *114* (8), 1733–1746.
- (3) Weng, Q.; Lu, D.; Schubring, J. Estimation of land surface temperature–vegetation abundance relationship for urban heat island studies. *Remote Sens. Environ.* **2004**, *89* (4), 467–483.
- (4) Li, Y.; Schubert, S.; Kropp, J. P.; Rybski, D. On the influence of density and morphology on the Urban Heat Island intensity. *Nat. Commun.* **2020**, *11* (1), 2647.

- (5) Zhao, S.; Liu, S.; Zhou, D. Prevalent vegetation growth enhancement in urban environment. *Proc. Natl. Acad. Sci. U. S. A.* **2016**, *113* (22), 6313–6318.
- (6) Wong, N. H.; Tan, C. L.; Kolokotsa, D. D.; Takebayashi, H. Greenery as a mitigation and adaptation strategy to urban heat. *Nat. Rev. Earth Environ.* **2021**, *2* (3), 166–181.
- (7) Harris, N. L.; Gibbs, D. A.; Baccini, A.; Birdsey, R. A.; De Bruin, S.; Farina, M.; Fatoyinbo, L.; Hansen, M. C.; Herold, M.; Houghton, R. A.; Potapov, P. V. Global maps of twenty-first century forest carbon fluxes. *Nat. Clim. Change* **2021**, *11* (3), 234–240.
- (8) Zhao, L.; Oleson, K.; Bou-Zeid, E.; Krayenhoff, E. S.; Bray, A.; Zhu, Q.; Zheng, Z.; Chen, C.; Oppenheimer, M. Global multi-model projections of local urban climates. *Nat. Clim. Change* **2021**, *11* (2), 152–157.
- (9) Bachir, N.; Bounoua, L.; Aiche, M.; Maliki, M.; Nigro, J.; El Ghazouani, L. The simulation of the impact of the spatial distribution of vegetation on the urban microclimate: A case study in Mostaganem. *Urban Climate* **2021**, *39*, 100976.
- (10) Xiao, X. D.; Dong, L.; Yan, H.; Yang, N.; Xiong, Y. The influence of the spatial characteristics of urban green space on the urban heat island effect in Suzhou Industrial Park. *Sustainable Cities Soc.* **2018**, *40*, 428–439.
- (11) Qiu, K.; Jia, B. The roles of landscape both inside the park and the surroundings in park cooling effect. *Sustainable Cities Soc.* **2020**, *52*, 101864.
- (12) He, C.; Zhang, Y.; Schneider, A.; Chen, R.; Zhang, Y.; Ma, W.; Kinney, P. L.; Kan, H. The inequality labor loss risk from future urban warming and adaptation strategies. *Nat. Commun.* **2022**, *13* (1), 3847.
- (13) Forzieri, G.; Alkama, R.; Miralles, D. G.; Cescatti, A. Satellites reveal contrasting responses of regional climate to the widespread greening of Earth. *Science* **2017**, *356* (6343), 1180–1184.
- (14) Li, Y.; Zeng, Z.; Huang, L.; Lian, X.; Piao, S. Comment on “Satellites reveal contrasting responses of regional climate to the widespread greening of Earth”. *Science* **2018**, *360* (6394), No. eaap7950.
- (15) Cook-Patton, S. C.; Gopalakrishna, T.; Daigneault, A.; Leavitt, S. M.; Platt, J.; Scull, S. M.; Amarjargal, O.; Ellis, P. W.; Griscom, B. W.; McGuire, J. L. Lower cost and more feasible options to restore forest cover in the contiguous United States for climate mitigation. *One Earth* **2020**, *3* (6), 739–752.
- (16) Song, S.; Ding, Y.; Li, W.; Meng, Y.; Zhou, J.; Gou, R.; Zhang, C.; Ye, S.; Saintilan, N.; Krauss, K. W. Mangrove reforestation provides greater blue carbon benefit than afforestation for mitigating global climate change. *Nat. Commun.* **2023**, *14* (1), 756.
- (17) Amelung, W.; Bossio, D.; de Vries, W.; Kögel-Knabner, I.; Lehmann, J.; Amundson, R.; Bol, R.; Collins, C.; Lal, R.; Leifeld, J. Towards a global-scale soil climate mitigation strategy. *Nat. Commun.* **2020**, *11* (1), 5427.
- (18) Betts, R. A. Afforestation cools more or less. *Nat. Geosci.* **2011**, *4* (8), 504–505.
- (19) Windisch, M. G.; Davin, E. L.; Seneviratne, S. I. Prioritizing reforestation based on biogeochemical and local biogeophysical impacts. *Nat. Clim. Change* **2021**, *11* (10), 867–871.
- (20) Arora, V. K.; Montenegro, A. Small temperature benefits provided by realistic afforestation efforts. *Nat. Geosci.* **2011**, *4* (8), 514–518.
- (21) Piao, S.; Wang, X.; Park, T.; Chen, C.; Lian, X.; He, Y.; Bjerke, J. W.; Chen, A.; Ciais, P.; Tømmervik, H. Characteristics, drivers and feedbacks of global greening. *Nat. Rev. Earth Environ.* **2020**, *1* (1), 14–27.
- (22) Chen, C.; Park, T.; Wang, X.; Piao, S.; Xu, B.; Chaturvedi, R. K.; Fuchs, R.; Brovkin, V.; Ciais, P.; Fensholt, R.; Tømmervik, H. China and India lead in greening of the world through land-use management. *Nat. Sustainability* **2019**, *2* (2), 122–129.
- (23) García-Lamarca, M.; Anguelovski, I.; Venner, K. Challenging the financial capture of urban greening. *Nat. Commun.* **2022**, *13* (1), 7132.
- (24) Zhang, L.; Yang, L.; Zohner, C. M.; Crowther, T. W.; Li, M.; Shen, F.; Guo, M.; Qin, J.; Yao, L.; Zhou, C. Direct and indirect impacts of urbanization on vegetation growth across the world’s cities. *Sci. Adv.* **2022**, *8* (27), No. eab0095.
- (25) Song, F.; Bao, J.; Li, T.; Yu, T.; Yuan, Y.; Huang, X.; Bao, A.; De Maeyer, P. Contrasting inequality of green spaces and buildings between cities in China. *Building Environ.* **2024**, *254*, 111384.
- (26) Wu, L.; Kim, S. K. Exploring the equality of accessing urban green spaces: A comparative study of 341 Chinese cities. *Ecol. Indic.* **2021**, *121*, 107080.
- (27) Wu, L.; Kim, S. K. Does socioeconomic development lead to more equal distribution of green space? Evidence from Chinese cities. *Sci. Total Environ.* **2021**, *757*, 143780.
- (28) Didan, K. MOD13Q1MODIS/Terra vegetation indices 16-day L3 global 250m SIN grid V006. *NASA Eosdis Land Processes Daac* **2015**, *10* 1.
- (29) Friedl, M.; Sulla-Menashe, D. MCD12Q1MODIS/Terra+ aqua land cover type yearly L3 global 500m SIN grid V006. *NASA Eosdis Land Processes Daac* **2019**, *10*, 200.
- (30) Wan, Z.; Hook, S.; Hulley, G. MOD11A2MODIS/Terra land surface temperature/emissivity 8-day L3 global 1km SIN grid V006. *NASA Eosdis Land Processes Daac* **2015**, *10*.
- (31) Vermote, E. MOD09A1MODIS/terra surface reflectance 8-day L3 global 500m SIN grid V006. *NASA Eosdis Land Processes Daac* **2015**, *10*.
- (32) Hersbach, H.; Bell, B.; Berrisford, P.; Hirahara, S.; Horányi, A.; Muñoz-Sabater, J.; Nicolas, J.; Peubey, C.; Radu, R.; Schepers, D.; Simmons, A. The ERA5 global reanalysis. *Quart J Royal Meteorol Soc.* **2020**, *146* (730), 1999–2049.
- (33) Tatem, A. J. WorldPop, open data for spatial demography. *Sci. Data* **2017**, *4* (1), 170004.
- (34) Gong, P.; Li, X.; Wang, J.; Bai, Y.; Chen, B.; Hu, T.; Liu, X.; Xu, B.; Yang, J.; Zhang, W. Annual maps of global artificial impervious area (GAIA) between 1985 and 2018. *Remote Sens. Environ.* **2020**, *236*, 111510.
- (35) Li, X.; Zhou, Y.; Zhao, M.; Zhao, X. A harmonized global nighttime light dataset 1992–2018. *Sci. Data* **2020**, *7* (1), 168.
- (36) Li, X.; Gong, P.; Zhou, Y.; Wang, J.; Bai, Y.; Chen, B.; Hu, T.; Xiao, Y.; Xu, B.; Yang, J.; Liu, X. Mapping global urban boundaries from the global artificial impervious area (GAIA) data. *Environ. Res. Lett.* **2020**, *15* (9), 094044.
- (37) Beck, H. E.; Zimmermann, N. E.; McVicar, T. R.; Vergopolan, N.; Berg, A.; Wood, E. F. Present and future Köppen-Geiger climate classification maps at 1-km resolution. *Sci. Data* **2018**, *5* (1), 180214.
- (38) Xu, H. A new index for delineating built-up land features in satellite imagery. *Int. J. Remote Sens.* **2008**, *29* (14), 4269–4276.
- (39) Savitzky, A.; Golay, M. J. Smoothing and differentiation of data by simplified least squares procedures. *Anal. Chem.* **1964**, *36* (8), 1627–1639.
- (40) Gorelick, N.; Hancher, M.; Dixon, M.; Ilyushchenko, S.; Thau, D.; Moore, R. Google Earth Engine: Planetary-scale geospatial analysis for everyone. *Remote Sens. Environ.* **2017**, *202*, 18–27.
- (41) Tett, S. F.; Stott, P. A.; Allen, M. R.; Ingram, W. J.; Mitchell, J. F. Causes of twentieth-century temperature change near the Earth’s surface. *Nature* **1999**, *399* (6736), 569–572.
- (42) Campbell, I. *Beating the heat: A sustainable Cooling Handbook for Cities* UN environment programme, 2021.
- (43) Hisdal, H.; Stahl, K.; Tallaksen, L. M.; Demuth, S. Have streamflow droughts in Europe become more severe or frequent? *Int. J. Climatol.* **2001**, *21* (3), 317–333.
- (44) Wu, H.; Soh, L.-K.; Samal, A.; Chen, X.-H. Trend analysis of streamflow drought events in Nebraska. *Water Resour. Manage.* **2008**, *22*, 145–164.
- (45) Peng, J.; Jia, J.; Liu, Y.; Li, H.; Wu, J. Seasonal contrast of the dominant factors for spatial distribution of land surface temperature in urban areas. *Remote Sens. Environ.* **2018**, *215*, 255–267.
- (46) Nemani, R. R.; Keeling, C. D.; Hashimoto, H.; Jolly, W. M.; Piper, S. C.; Tucker, C. J.; Myneni, R. B.; Running, S. W. Climate-driven increases in global terrestrial net primary production from 1982 to 1999. *Science* **2003**, *300* (5625), 1560–1563.
- (47) Zeng, Z.; Piao, S.; Li, L. Z.; Zhou, L.; Ciais, P.; Wang, T.; Li, Y.; Lian, X.; Wood, E. F.; Friedlingstein, P.; Mao, J. Climate mitigation

from vegetation biophysical feedbacks during the past three decades. *Nat. Clim. Change* **2017**, *7* (6), 432–436.

(48) Upadhyay, R.; Wang, Z.-H.; Yang, J. Radiative shading effect of urban trees on cooling the regional built environment. *Urban Forestry Urban Greening* **2017**, *26*, 18–24.

(49) Cuthbert, M. O.; Rau, G.; Ekström, M.; O'Carroll, D.; Bates, A. Global climate-driven trade-offs between the water retention and cooling benefits of urban greening. *Nat. Commun.* **2022**, *13* (1), 518.

(50) Sun, L.; Chen, J.; Li, Q.; Huang, D. Dramatic uneven urbanization of large cities throughout the world in recent decades. *Nat. Commun.* **2020**, *11* (1), 5366.

(51) Estoque, R. C.; Murayama, Y.; Myint, S. W. Effects of landscape composition and pattern on land surface temperature: An urban heat island study in the megacities of Southeast Asia. *Sci. Total Environ.* **2017**, *577*, 349–359.

(52) Antrop, M. Landscape change and the urbanization process in Europe. *Landscape Urban Plann.* **2004**, *67* (1–4), 9–26.

(53) Kaika, D.; Zervas, E. The Environmental Kuznets Curve (EKC) theory—Part A: Concept, causes and the CO₂ emissions case. *Energy Policy* **2013**, *62*, 1392–1402.

(54) Chan, E.; Lee, G. K. Critical factors for improving social sustainability of urban renewal projects. *Soc. Indicat. Res.* **2007**, *85*, 243–256.

(55) Li, Y.; Li, Z.-L.; Wu, H.; Zhou, C.; Liu, X.; Leng, P.; Yang, P.; Wu, W.; Tang, R.; Shang, G.-F. Biophysical impacts of earth greening can substantially mitigate regional land surface temperature warming. *Nat. Commun.* **2023**, *14* (1), 121.

(56) Rohatyn, S.; Yakir, D.; Rotenberg, E.; Carmel, Y. Limited climate change mitigation potential through forestation of the vast dryland regions. *Science* **2022**, *377* (6613), 1436–1439.

(57) Schleussner, C.-F.; Rogelj, J.; Schaeffer, M.; Lissner, T.; Licker, R.; Fischer, E. M.; Knutti, R.; Levermann, A.; Frieler, K.; Hare, W. Science and policy characteristics of the Paris Agreement temperature goal. *Nat. Clim. Change* **2016**, *6* (9), 827–835.

(58) Walther, G.-R.; Post, E.; Convey, P.; Menzel, A.; Parmesan, C.; Beebee, T. J.; Fromentin, J.-M.; Hoegh-Guldberg, O.; Bairlein, F. Ecological responses to recent climate change. *Nature* **2002**, *416* (6879), 389–395.

(59) Lloret, F.; Escudero, A.; Iriondo, J. M.; Martínez-Vilalta, J.; Valladares, F. Extreme climatic events and vegetation: the role of stabilizing processes. *Global Change Biol.* **2012**, *18* (3), 797–805.

(60) Anderegg, W. R.; Trugman, A. T.; Badgley, G.; Anderson, C. M.; Bartuska, A.; Ciais, P.; Cullenward, D.; Field, C. B.; Freeman, J.; Goetz, S. J. Climate-driven risks to the climate mitigation potential of forests. *Science* **2020**, *368* (6497), No. eaaz7005.

(61) Alkama, R.; Forzieri, G.; Duveiller, G.; Grassi, G.; Liang, S.; Cescatti, A. Vegetation-based climate mitigation in a warmer and greener World. *Nat. Commun.* **2022**, *13* (1), 606.

(62) Akuraju, V.; Pradhan, P.; Haase, D.; Kropp, J. P.; Rybski, D. Relating SDG11 indicators and urban scaling—An exploratory study. *Sustainable Cities Soc.* **2020**, *52*, 101853.

(63) Lu, N.; Tian, H.; Fu, B.; Yu, H.; Piao, S.; Chen, S.; Li, Y.; Li, X.; Wang, M.; Li, Z. Biophysical and economic constraints on China's natural climate solutions. *Nat. Clim. Change* **2022**, *12* (9), 847–853.

(64) Cook-Patton, S. C.; Drever, C. R.; Griscom, B. W.; Hamrick, K.; Hardman, H.; Kroeger, T.; Pacheco, P.; Raghav, S.; Stevenson, M.; Webb, C. Protect, manage and then restore lands for climate mitigation. *Nat. Clim. Change* **2021**, *11* (12), 1027–1034.

(65) Yu, L.; Xue, Y.; Diallo, I. Vegetation greening in China and its effect on summer regional climate. *Sci. Bull.* **2021**, *66* (1), 13–17.

(66) Chen, C.; Li, D.; Li, Y.; Piao, S.; Wang, X.; Huang, M.; Gentile, P.; Nemani, R. R.; Myneni, R. B. Biophysical impacts of Earth greening largely controlled by aerodynamic resistance. *Sci. Adv.* **2020**, *6* (47), No. eabb1981.

(67) Zhang, T.; Zhou, Y.; Zhao, K.; Zhu, Z.; Chen, G.; Hu, J.; Wang, L. A global dataset of daily near-surface air temperature at 1-km resolution (2003–2020). *Earth Syst. Sci. Data Discuss.* **2022**, *14*, 5637–5649.